*Desalination and Water Treatment*
www.deswater.com

doi: 10.5004/dwt.2021.27428

230 (2021) 184–192
August

# Performance improvement of reduced graphene oxide blended PVDF ultrafiltration membrane

Khira Zlaoui[a,b], Asma Rhimi[a,c], Dorra Jellouli Ennigrou[a,*], Karima Horchani Naifer[a]

[a]*Physical Chemistry Laboratory of Mineral Materials and their Applications, National Center for Research in Materials Sciences, Technopark Borj Cedria, P.O. Box: 73-8027, Soliman, Tunisia, Tel. (+216) 79 32 52 50/(+216) 79 32 52 80; emails: ennigrou2@gmail.com (D.J. Ennigrou), khira.zlaoui@gmail.com (K. Zlaoui), asmarhimi2014@gmail.com (A. Rhimi), karima_horchani@yahoo.com (K.H. Naifer)*
[b]*Faculty of Sciences of Bizerte, Bizerte, Tunisia*
[c]*Faculty of Sciences of Tunis, Tunis, Tunisia*

Received 16 February 2021; Accepted 12 May 2021

**ABSTRACT**

The performance of a novel polyvinylidene fluoride (PVDF) membrane with high hydrophilicity and enhanced separation ability was discussed with the addition of a small amount of reduced graphene oxide nanoparticles (rGO). The PVDF-rGO ultrafiltration composite membrane was effectively synthesized, by incorporating rGO (0.1% wt) as nanoparticles by the phase inversion process. The impact of these modifications was studied. The morphological structure of the membranes was evaluated by scanning electron microscopy (SEM). The changes in the chemical structure were investigated using Fourier-transform infrared spectroscopy. The SEM images revealed that in the PVDF membrane, the diameter of the pores increased after rGO grafting. Performance tests showed that the PVDF membrane has flux and a rejection of bovine serum albumin about 92% at an optimum transmembrane pressure of 4 bar. The incorporation of rGO improved the protein rejection, reaching a rejection rate of around 92% at 4 bar. These results suggest that incorporating rGO nanoparticles can enhance the permeability of the membrane. The PVDF membrane modified with 0.1 wt.% rGO showed a considerably higher flux than the unmodified membrane.

*Keywords:* PVDF membrane; Reduced graphene oxide; Ultrafiltration; rGO synthesis; Hydrophilicity

## 1. Introduction

Among the different inorganic materials, carbon nanoparticles are most commonly inserted into polymer matrix during ultrafiltration membranes preparation [1,2]. Recently, reduced graphene oxide (rGO) has acquired great importance due to its exceptional structural, chemical, and electrical properties [3–13]. In fact, it consists of a two-dimensional carbon monolayer made up of sp2 hybrided carbon atoms [14–18]. Graphene oxide nanosheets are applied for technological applications, such as energy storage, solar cells, and more recently for filtration membranes.

Graphene oxide nanomaterials present negatively charged defective sites, which might be counterbalanced by the presence of a proton, suggesting a separation efficacity in aqueous filtration [18]. Therefore, incorporating carbon nanoparticles into the polymer matrix (up to 10% of polymer weight) could provoke fewer defects in the nanocomposite membranes than other types of inorganic additives [19]. Indeed, they can improve the nanoporosity and reverse osmosis membrane

* Corresponding author.

fouling. Furthermore, they can improve permeability and salt rejection, in particular for seawater desalination [20].

The rGO nanoparticles are known for their hydrophilicity and high pore size, indicating the strong adsorption and rapid diffusion of water into the nanostructure which enhances water flux [21].

The rGO nanoparticles are considered as one of the most widely used materials for the polyvinylidene fluoride (PVDF) ultrafiltration membrane synthesis, thanks to antioxidant stability and good mechanical characteristics.

Thermodynamic compatibility of PVDF with rGO in terms of the interaction parameter. In fact, thermogravimetric analysis shows that the poly(ethyl methacrylate) (PEMA) likely PVDF [22] begins to decompose at around 230°C. Due to the thermal instability of PVDF, the heat treatment of the mixtures was limited to a maximum of 250°C. PVDF is a polymer with a solubility parameter closer to PAN [23] therefore it is miscible with PVP and DMAc. The choice of additives was also supported by the study made by Rana and Mandal [24], which describes the kinetics of the reverse emulsion photopolymerization of acrylamide using the solubility in water. Indeed, the synthesis protocol is similar and uses almost the same solvents.

Furthermore, the hydrophilic nature of PVDF seems to have the ability to absorb the organic component of the initial solution, leading to its contamination with proteins and other soils during the wastewater filtration process. This contamination, known as membrane fouling, results in a rapid decrease in the flux of pure water through the membranes [25]. In various researches, membrane fouling is seriously related to the surface microstructure and hydrophilicity [4]. Recently, researchers have focused on improving the surface hydrophilicity and the PVDF membrane fouling the incorporation of nanoparticles [26–28]. In particular, modifying the PVDF membrane by blending mineral materials is an efficient technique. The incorporation of properly dispersed inorganic nanoparticles into polymers at low concentrations improves membrane permeability and fouling [29]. Ultrafiltration is generally used in different fields such as food industries, oil-water separation, and protein purification [30].

Most studies on PVDF-rGO membranes have focused on modifying the UF and MF membranes. Liu et al. [31] prepared a thin-film nanocomposite hollow fiber membrane containing nanoparticles on the double-layer hollow fiber substrate such as PES and PVDF membranes.

The objective of this study is to synthesize a PVDF membrane mixed with rGO nanoparticles at a low concentration (0.1% wt.) to improve the hydrophilicity and separation performance.

## 2. Experimental

### 2.1. Materials

PVDF with an average molecular weight ($M_w$) of about 37 × 104 g/mol, dimethyl acetamide (DMAc), polyvinyl pyrrolidone (PVP), bovine serum albumin (BSA, $M_w$ of about 66 × 103 g/mol, and purity ≥ 96%) were purchased from Solvay advanced polymer. We synthesized the reduced graphene oxide (rGO) by modified Hummer's method with an average particle size of 0.45 μm.

A Milli-Q water purification system was used for the prepared solutions. All chemicals were used as received without further purification.

### 2.2. rGO nanoparticles synthesis

GO nanoparticle synthesis was previously detailed by Riahi et al. [32]. In this study, we opted to synthetize rGO monolayers in order to ensure material homogeneity. For that purpose, the collected raw material was suspended in ultrapure water under mechanical stirring and sonication many times and at different speeds. The mixture still contained graphite and visible multilayers in suspension as shown in Fig. 1.

These heavier particles were easily removed using centrifugation then filtered under vacuum using nylon membranes of different porosities to further homogenize the collected fractions and to determine particle size in each fraction. Fraction 1 was filtered using a first membrane with pores of 2.5 μm in order to remove large visible particles. The collected solution was immediately filtered through a second membrane with smaller pores (0.7 μm). Thus, the collected material through the second membrane has a dimension of between 2.5 and 0.7 μm. After lyophilization, a yield of 90% rGO monolayers was obtained with lateral dimensions between 2.5 and 0.45 μm (fraction 1: 2.1 g – fraction 2: 1.8 g, and fraction 3: 1.4 g).

### 2.3. Preparation of PVDF-rGO membrane

Table 1 describes the mixed solutions for the prepared membrane with different percentages of compounds. Solutions were stirred for about 5 h at room temperature (25°C) to ensure homogeneity. Then, the reduced graphene oxide rGo nanoparticles (0.1% wt.) were suspended in distilled water under ultrasonication for 3 d and heated at 70°C.

To obtain the PVDF-rGO membrane, the total solution was mixed homogeneously in one beaker under magnetic stirring for 48 h and heated at 60°C. The compound was cast by a doctor blade as shown in Fig. 2 and completely dried at room temperature in a bath of distilled water. A dried thin film of PVDF-rGO was obtained.

Membrane thickness was estimated with SEM. Fig. 2 describes the synthesis process of the two membranes. The developed membranes must be crosslinked before use in the filtration process.

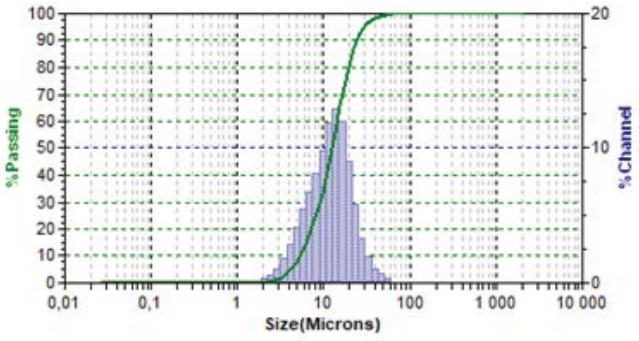


Fig. 1. Average rGO particle size.

### 2.4. Characterizations of rGO nanoparticles and membranes

#### 2.4.1. SEM analysis

The SEM technique (Quanta FEG 650) was used to identify the morphology of the rGO nanoparticles, the pore size, and the thickness of the membrane.

#### 2.4.2. Differential scanning calorimetry

Differential scanning calorimetry (DSC) calorimetry (a Mettler Toledo DSC823e, Germany) was used under the temperature range of 30°C –500°C. In order to obtain the DSC curves, samples were introduced in an aluminum crucible at a 10°C/min heating rate.

#### 2.4.3. Infrared spectrophotometric analysis (FTIR)

The chemical groups of the rGO nanoparticles and the synthesized membranes were identified by infrared spectroscopy – Fourier transforms infrared (FTIR) in a Frontier FT-IR spectrometer, model Perkin Elmer (France) equipped with the FTIR ATR accessory between 400 and 4,000 $cm^{-1}$ at 25°C. It studied the interaction between the groups of PVDF hydroxyl and determine the existence of hydrogen bonds between rGO and PVDF.

#### 2.4.4. Porosity

The gravimetric method was employed to determine the porosity of the synthesized membranes. $\varepsilon_m$ was calculated by the following equation:

$$\varepsilon_m = \left[\frac{\left(W_1 - W_2 / D_S\right)}{\left(W_1 - W_2 / D_S\right)} + \frac{W_2}{D_P}\right] \quad (1)$$

Table 1
The prepared membrane with different percentage of compounds

| Solutions | Membrane PVDF | Membrane PVDF-rGO |
|---|---|---|
| PVDF (wt.%) | 17 | 17 |
| PVP (wt.%) | 5 | 5 |
| DMAc (wt.%) | 18 | 17.9 |
| rGO (wt.%) | 0 | 0.1 |
| UP (ultrapure water) (wt.%) | 60 | 60 |
| Temperature of stirring (°C) | 70 | 70 |

where $W_1$, $W_2$ are the weights of the wet and the dry membrane respectively. $D_S$, $D_P$ are the solvent and the polymer density, respectively.

#### 2.4.5. Zeta-potential measurements

The zeta potential measurement (model: EKA, Brookhaven) was used to determine the surface charge of the synthesized membrane using an electrokinetic analyzer. The zeta potential was measured along the surface of the membrane. Two salts, NaCl and $Na_2SO_4$ were used in the range of 0.001–0.1 M concentration (20°C, pH = 7).

#### 2.4.6. Contact angle determination

A contact angle goniometer (OCA20, Data Physics Instruments, Germany) at room temperature was used to measure the contact angle of a DI water droplet on the membrane surface before and after modification with rGO nanoparticles. Before testing, the membranes were dried overnight at 50°C.

### 2.5. Filtration performance

The ultrafiltration unit was carried out in our laboratory to measure water flux and BSA recovery. The membrane with an effective area of 14.5 $cm^2$ was applied to the cell as shown in Fig. 3. The equipment consists of a cross-flow filtration cell with a pressure regulator (6 bar max).

Fig. 3. Filtration unit.

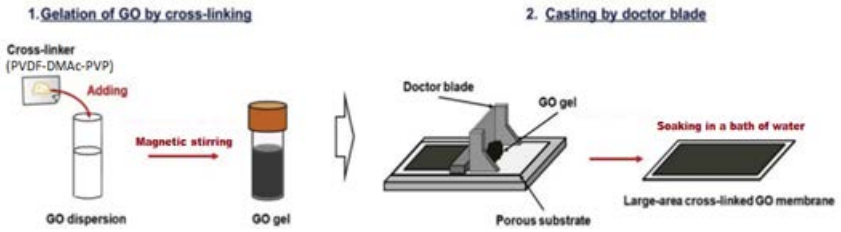


Fig. 2. Preparation of PVDF-rGO membrane by cross-linking [33].

#### 2.5.1. Water flux measurements

Each experiment started at a constant flow rate of 15 mL/min, by applying a transmembrane pressure between 1 and 6 bar. Ultrafiltration experiments were carried out at 25°C. The samples for analysis were collected at the inlet (ultrapure water) and the permeate.

The permeation flux $J_v$ (L/m²h) was calculated using the equation below:

$$J_v = \frac{V_p}{(A \times t)} \tag{2}$$

where $J_v$ is the permeation flux (L/m² h), $V_p$ (L) represents the volume of the permeate water collected over a period of time $t$ (h) through an active surface of membrane $A$ (m²).

The ultrapure water flux through the membrane at a variable transmembrane pressure is usually expressed with Darcy's law:

$$J_v = \frac{\Delta P_m}{\eta R_m} = L_p^0 \cdot \Delta P_m \tag{3}$$

where $L_p^0$ is the aqueous solution permeability, $\Delta P_m$ (bar) is the transmembrane pressure, and $R_m$ is the hydraulic membrane resistance.

#### 2.5.2. Rejection under the transmembrane pressure

Protein solutions were prepared one hour before use and stored at 4°C to ensure that BSA molecules were still active and that there was no bacterial contamination. The feed transmembrane pressure was controlled in the range of 1–6 bar and the filtration process was carried out by filtering 15 mL of protein solution through the membranes at ambient conditions.

The solution of BSA was prepared (1 g/L and pH = 7). The permeate and feed solutions were determined by optical absorption at 298 nm, corresponding to the maximum value for the protein.

The evaluation of the BSA retention $R$ (%) was determined by the equation below:

$$R(\%) = \left(1 - \frac{C_p}{C_f}\right) \times 100 \tag{4}$$

where $C_p$ and $C_f$ are BSA and feed concentrations (g/L), respectively.

## 3. Results and discussions

### 3.1. Characterization of rGO nanoparticles

X-ray diffractogram (XRD) of graphite, GO and rGO nanoparticles is shown in Fig. 4. The peak of graphite is located at 2θ = 25.72°, which indicates that the crystallinity is high. The diffraction peak of GO is at 2θ = 9.5° corresponding to the $d$-spacing of GO which is 0.85 nm. The existence of oxygen functional groups and water molecules in the layers may be due to the increase in $d$-spacing.

The diffraction peaks completely disappeared, indicating that the graphite powders were totally oxidized following the reduction. This may be due to the rGO formation in the reduction time.

In Fig. 5, the Raman spectra show that the following peaks at 1,336 and 1,595 cm$^{-1}$ may be due to the presence of impurity and the graphitic carbon atom in the carbon lattice [34]. Furthermore, the two peaks and the ratio (1.20) demonstrate that the rGO was successfully synthesized.

On the other hand, Fig. 6 depicts FT-IR spectra of the graphite, GO, and rGO. The three powders demonstrated peaks at 3,417; 1,408; and 1,062 cm$^{-1}$ due to the presence of functional groups of O–H, C–O, and epoxy, respectively. The peak intensity of 1,062 cm$^{-1}$ decreased in the rGO spectrum. In general, the FT-IR spectra reveal the same graphite, GO, and rGO peaks [35]. SEM analysis in Fig. 7 displays the morphology of the rGO nanoparticles, which shows that rGO reveals a nanosheet structure similar to that of reduced graphene oxide [36]. The dispersion of carbon on the surface may cause a decrease in the repartition of rGO nanosheets.

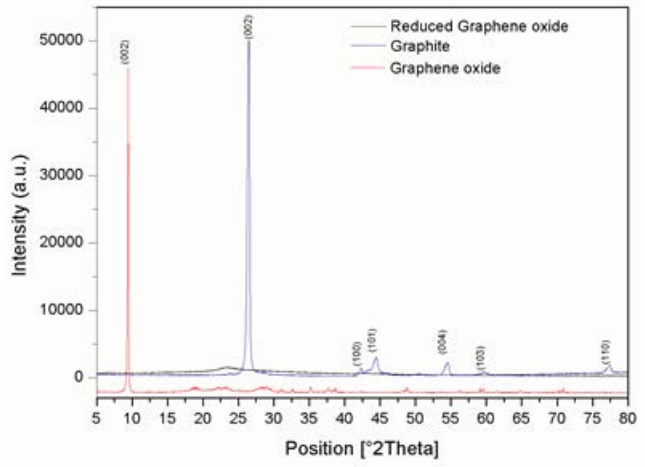


Fig. 4. X-ray diffractogram of graphite, GO, and rGO nanoparticles.

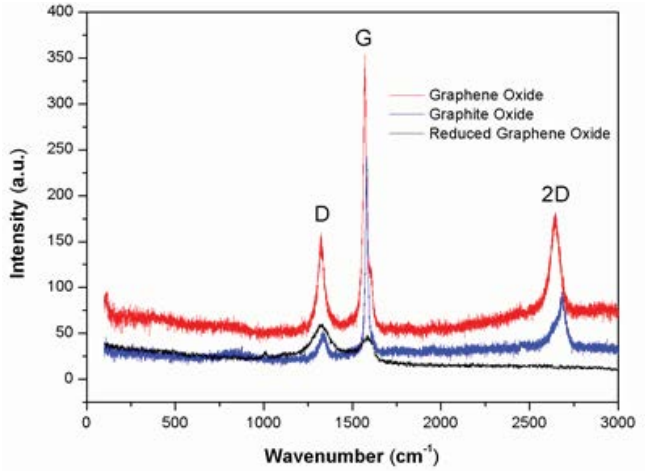


Fig. 5. Raman spectra of graphite, GO, and rGO nanoparticles.

### 3.2. Characterizations of PVDF and PVDF/rGO membranes

After the addition of the rGO, the surface of the PVDF membrane (Fig. 8a and b) becomes smoother. Thus, its addition is not visible in the SEM, indicating that it is well-dispersed. Besides the cross-section of the membrane by the SEM, it can be clearly seen the presence of a column-like structure of the PVDF-rGO membrane. The addition of rGO has improved the dispersion of the membrane additives by interacting with the oxygen groups. Too much rGO addition (>0.1% wt.) could clog the membrane.

The FTIR spectra (Fig. 9) show that the two membranes have the same spectra. The $CH_2$ groups are characteristic of the peak located at 3,024 $cm^{-1}$. However, the peak located at 1,640 $cm^{-1}$ is attributed to the CONH groups from the DMAc in the initial compound. The peak at 1,117 $cm^{-1}$ matches with the $CF_2$ stretching vibration of PVDF chains. The enlargement of the two hydrophilic groups (OH and CH); observed at 3,400 and 841 $cm^{-1}$, improves the hydrophilicity of the composite membrane by the rGO blending [37].

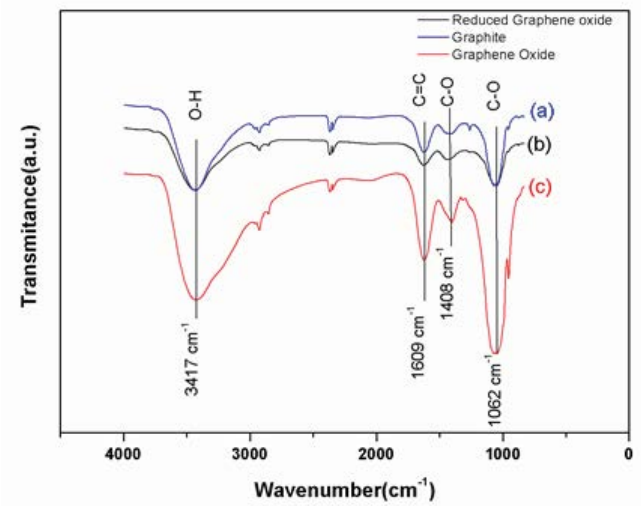


Fig. 6. FTIR spectra of graphite, GO, and rGO nanoparticles.

The DSC curve of the obtained membranes is presented in Fig. 10. Fig. 10 shows an endothermic peak for the two membranes at around 165°C. The DSC curves reveal that both two membranes are stable [38].

PVDF-rGO pores ranged from 10 to 20 nm for the PVDF membrane [39–41] and 15–18 nm for the PVDF-rGO [42].

Fig. 11 shows the water contact angle of PVDF and rGO-PVDF membranes. The contact angle decreased from 85.6° (PVDF membrane) to 50.76° when adding the rGO nanoparticles, which indicates an improvement of the membrane with the suitable amount of rGO. This may be due to the oxygen groups on the surface, which interact easily with molecules of water, enhancing the hydrophilicity of the membrane [43].

In fact, a decrease in contact angle leads to an increase in the size of pores in the membrane as well as permeability. The basic properties related to the contact angle are the permeability of pure water, porosity, and pore size. The super hydrophilic nature of rGO and its high affinity to water led to the enhancement of hydrophilicity in the membrane. Excessive addition of rGO may cause agglomeration, which blocks the pores of the membrane [44].

Previous studies show that excessive addition of carbon nanotubes (over 0.2 wt.%) reduces the energy of the surface of the membrane. It can affect hydrophilicity by reducing and even blocking the pores [45]. Thus, the choice of the 0.1% wt. rGO addition in the PVDF membrane leads to better hydrophilicity.

### 3.3. Effect of water and BSA fluxes on the membranes

Fig. 12a and b show the permeate fluxes of pure water and BSA as a function of transmembrane pressure $\Delta P$ through the membranes, respectively. Permeate fluxes increased when the transmembrane pressure increased from 1 to 6 bar, as expected by Eq. (3).

The slopes are the membrane permeabilities of pure water (Fig. 12a) and BSA (Fig. 12b).

As shown in Table 2, the zeta potential decreased. This can be explained by the functional groups of rGO nanoparticles, which led to the enhancement of the hydrophilicity

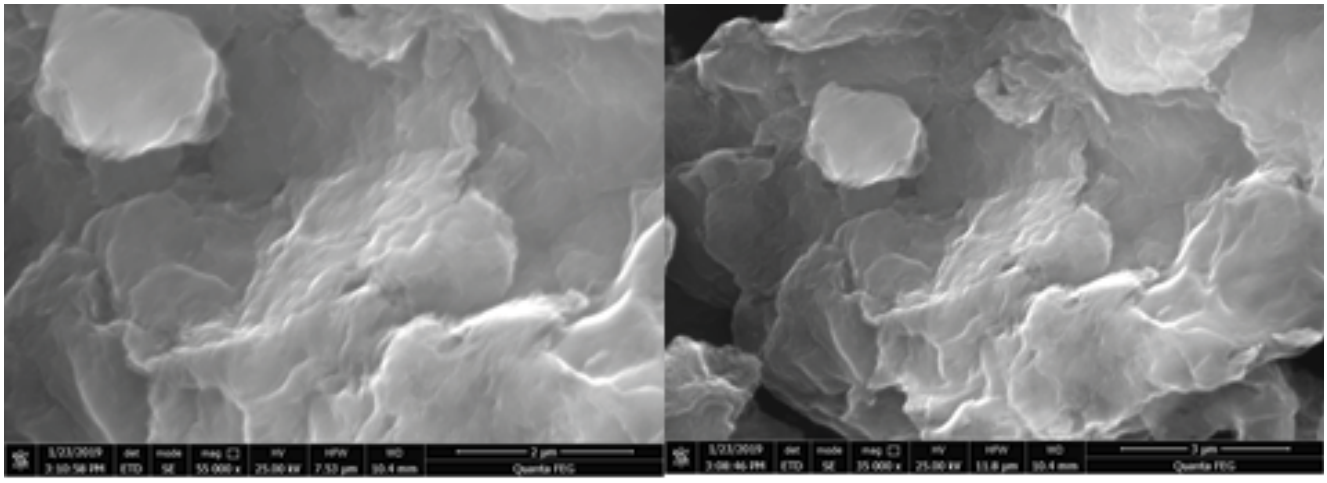

Fig. 7. SEM images of rGO.

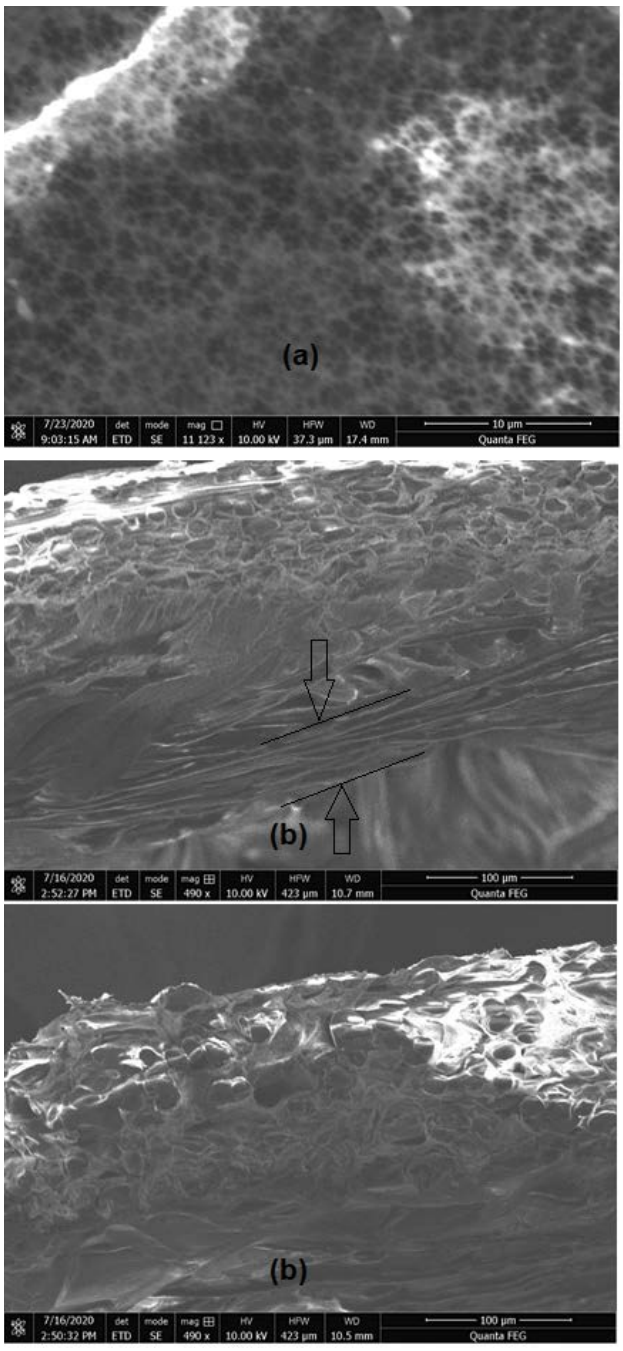


Fig. 8. Transversal and cross-sectional SEM images of (a) pristine PVDF membrane and (b) rGO/PVDF membrane.

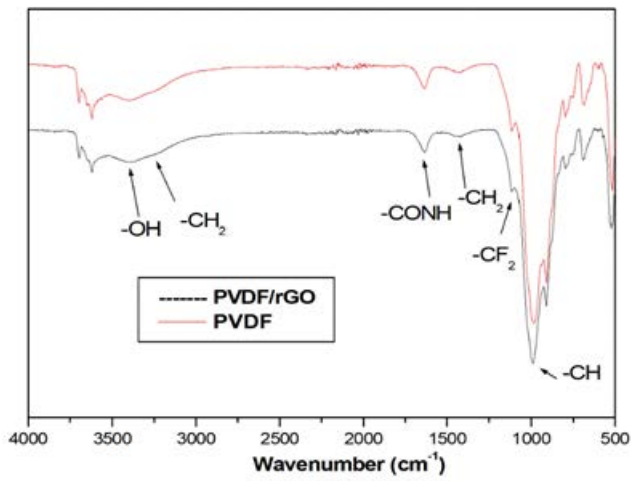


Fig. 9. FTIR spectra of PVDF and PVDF/rGO membranes.

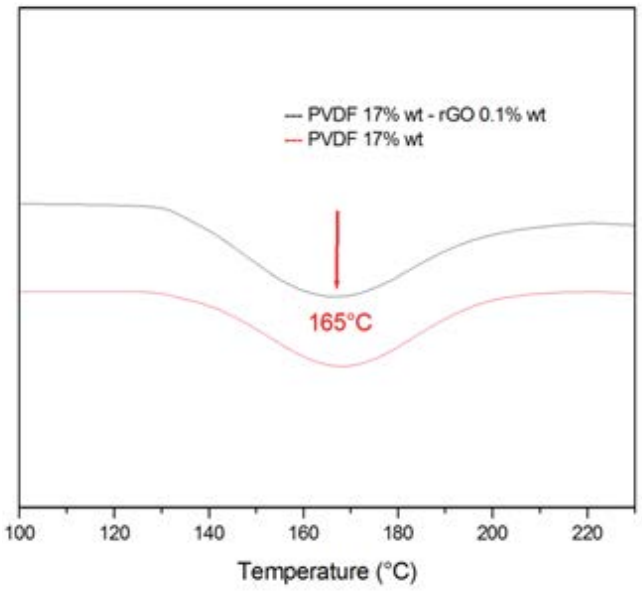


Fig. 10. DSC curves of the membranes PVDF-17 and PVDF-17/rGO-0.1 wt.%.

and the increasing of the negative charge on the surface of the membrane [46].

The coating of the rGO nanoparticles on the membrane is well-identified by SEM images (Fig. 8b). The fluxes of the membranes are affected by their hydrophilicity and it can be observed in Fig. 12a and b, that pure water fluxes of PVDF-rGO membrane are higher than that of PVDF one. In fact, the mass transfer of water can be enhanced by the addition of rGO nanoparticles in the membrane, controlling the hydrogen bonds and accelerating the rate of transfer of water. The improvement of the membrane surface is directly related to the enhancement of its hydrophilicity.

The transfer rate of water molecules and the mass transfer resistance is improved by the addition of carbon nanotubes.

The fluxes of BSA decreased compared to the water fluxes and this is due to the largest molecular weight of this protein. The addition of rGO nanoparticles into the membrane improves the diffusion of water into the pores. The adherence to the surface of the membrane is well improved [43,45]. Excessive addition of rGO could block the pores of the membrane. This could justify our choice of adding 0.1 wt.% of rGO into the mixture of the PVDF membrane.

Table 2
Pure water permeabilities and physical characteristics of PVDF and PVDF-rGO membranes

| Membrane | Contact angle | Zeta potential (mV) at pH = 7 | Thickness (μm) | $L_p^0$ (water) (L/h m$^2$ bar) | $L_p$ (BSA) (L/h m$^2$ bar) |
|---|---|---|---|---|---|
| PVDF | 85.60 | –8.83 ± 3.5 | 0.053 | 16.24 | 5.64 |
| PVDF-rGO 0.1 | 50.76 | –37.81 ± 4 | 0.048 | 20.25 | 10.56 |

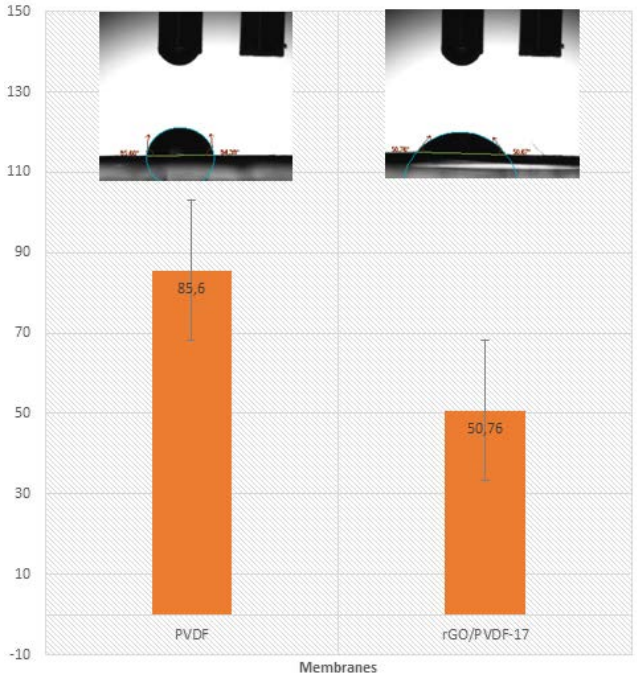


Fig. 11. Water contact angles of PVDF membranes with and without rGO.

### 3.4. BSA removal on the synthesized membranes

As shown in Fig. 6, the retention of BSA is better compared to the PVDF membrane. Indeed, the rGO nanoparticles are considered to be hydrophilic particles and thus improve the anti-fouling properties of the PVDF-rGO membrane. With multiple uses, the PVDF-rGO membrane would keep the same anti-fouling properties.

The interaction of the membrane with water molecules is enhanced by the incorporation of the rGO. In the PVDF matrix, this is thanks to the hydrophilic properties of these nanoparticles, which leads to improved BSA rejection. In the PVDF membrane, cleaning only partially removes the membrane after use, and this because of the collimating of BSA in its pores. On the other hand, thanks to the interaction between the water molecules and the rGO nanoparticles by the hydrogen bonds, this prevents the presentation of BSA in the pores of the PVDF-rGO membrane. Accordingly, the rGO nanoparticles are conductive in the ambient [29] and that enhances the properties of PVDF membranes by their addition.

Other studies indicate that excessive addition of nanoparticles leads to blockage of the membrane pores. This is accentuated by the results obtained from the pores of the membrane synthesized [42]. This explains our choice of the percentage of rGO nanoparticles added to the PVDF membrane.

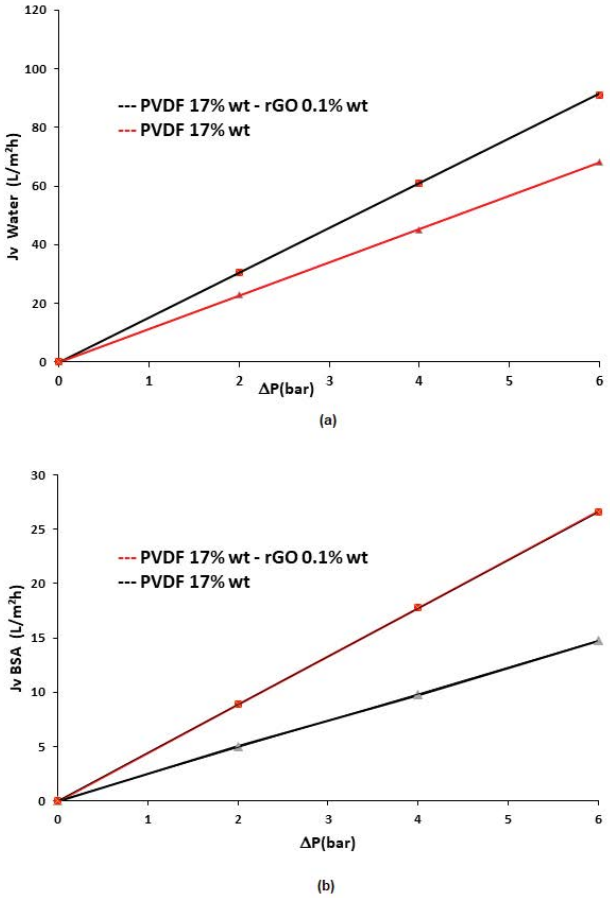


Fig. 12. Permeate flux of: (a) pure water as a function of transmembrane pressure and (b) BSA as a function of transmembrane pressure, [BSA] = 1 g/L.

Fig. 13 depicts the variation as a function of the transmembrane pressure for a feed protein concentration of 1 g/L at 25°C. It shows that the BSA retention reached nearly ~92% at 4 bar for the PVDF-rGO membrane. Above 4 bar, the rejection of BSA decreased for all membranes and reached 70% at 2 bar. Therefore, the optimum pressure is 4 bar at the ambient. It shows that the BSA retention reached nearly ~92% at 4 bar for the PVDF-rGO membrane.

BSA retention is described by Fig. 13 as a function of the transmembrane pressure for BSA at 1 g/L.

## 4. Conclusion

This work reports the addition of 1% wt. of rGO into PVDF membrane casting with Doctor Blade. The rGO

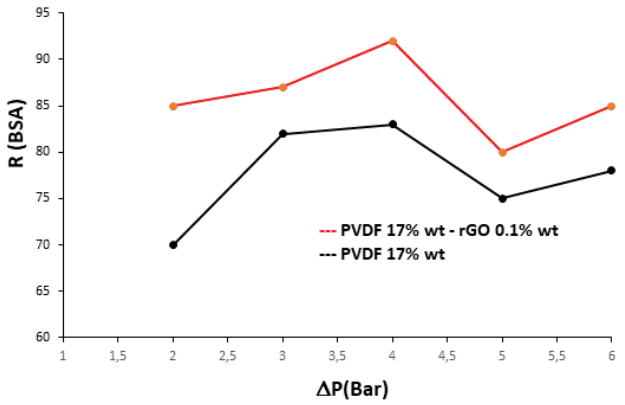


Fig. 13. BSA retention as a function of transmembrane pressure, [BSA] = 1 g/L.

nanoparticles are considered hydrophilic particles which ameliorate the hydrophilicity and improve the separation performance when added to the PVDF membrane.

The PVDF membrane is characteristic of a rough surface and the addition of rGO improves the membrane surface as observed in the SEM images. Excessive addition of rGO has a negative effect on the membrane. In fact, 0.1% wt. of rGO has the better porosity and can enhance the hydrophilicity the permeability, and retention of BSA.

SEM confirmed the homogeneity of the synthesized PVDF-rGO membrane. The decrease in the contact angle has a direct effect on the improvement of the physicochemical properties of the PVDF membrane (thermal stability, homogeneity, and good pore distribution). Permeability and BSA antifouling experiments for PVDF and PVDF/rGO membranes showed that the PVDF/rGO membrane has a higher pure water flux and BSA retention than those of the pristine PVDF membrane.

RGO incorporation into the PVDF matrix would lead to enhanced hydrophilicity and antifouling performance.

## References


[1] H. Song, J. Shao, J. Wang, X. Zhong, The removal of natural organic matter with LiCl–$TiO_2$-doped PVDF membranes by integration of ultrafiltration with photocatalysis, Desalination, 344 (2014) 412–421.

[2] Q. Wu, G.E. Chen, W.G. Sun, Z.L. Xu, Y.F. Kong, X.P. Zheng, S.J. Xu, Bio-inspired GO-Ag/PVDF/F127 membrane with improved anti-fouling for natural organic matter (NOM) resistance, Chem. Eng. J., 313 (2017) 450–460.

[3] W.S. Hummers, R.E. Offeman, Preparation of graphitic oxide, J. Am. Chem. Soc., 80 (1958) 1339, doi: 10.1021/ja01539a017.

[4] Y. Wang, Z. Mo, P. Zhang, C. Zhang, L. Han, R. Guo, H. Gou, X. Wei, R. Hu, Synthesis of flower-like $TiO_2$ microsphere/graphene composite for removal of organic dye from water, Mater. Des., 99 (2016) 378–388.

[5] H.N. Lim, N.M. Huang, C.H. Loo, Facile preparation of graphene-based chitosan films: enhanced thermal, mechanical and antibacterial properties, J. Non-Cryst. Solids, 358 (2012) 525–530.

[6] R.V. Brade, S.A. Waghuley, Preparation and electrical conductivity of novel vanadate borate glass system containing graphene oxide, J. Non-Cryst. Solids, 376 (2013) 117–125.

[7] A. Bonanni, M. Pumera, High-resolution impedance spectroscopy for graphene characterization, Electrochem. Commun., 26 (2013) 52–54.

[8] A.H. Castro Neto, F. Guinea, N.M.R. Peres, K.S. Novoselov, A.K. Geim, The electronic properties of graphene, Rev. Mod. Phys., 81 (2009) 109–162, doi: 10.1103/RevModPhys.81.109.

[9] L. Shen, S. Xiong, Y. Wang, Graphene oxide incorporated thin-film composite membranes for forward osmosis applications, Chem. Eng. Sci., 143 (2016) 194–205.

[10] X.J. Kang, J.M. Zhang, X.W. Sun, F.R. Zhang, Y.X. Zhang, One-pot synthesis of vanadium dioxide nanoflowers on graphene oxide, Ceram. Int., 42 (2016) 7883–7887.

[11] J. Munoz, R. Montes, M. Baeza, Trends in electrochemical impedance spectroscopy involving nanocomposite transducers: characterization, architecture surface and bio-sensing, TrAC, Trends Anal. Chem., 97 (2017) 201–215.

[12] G.R. Ferbandez, M.C. Rodriguez, A. Arenillas, J.A. Menéndez, I. da Rodríguez-Pastor, I. Martin-Gullon, Determinant influence of the electrical conductivity versus surface area on the performance of graphene oxide-doped carbon xerogel supercapacitors, Carbon, 126 (2018) 456–463.

[13] J.C. Meyer, A.K. Geim, M.I. Katselson, K.S. Novoselov, D. Obergfell, S. Roth, C.Girit, A. Zettl, On the roughness of single- and bilayer graphene membranes, Solid State Commun., 143 (2007) 101–109.

[14] R.P. Bustamante, D.B. Morales, J.B. Martinez, I. Estrada-Guel, R. Martínez-Sánchez, Microstructural and hardness behavior of graphene-nanoplatelets/aluminum composites synthesized by mechanical alloying, J. Alloys Compd., 615 (2014) 5578–5582.

[15] O. Jankovsky, P. Simek, D. Sedminubky, S. Huber, M. Pumer, Z. Sofer, Towards highly electrically conductive and thermally insulating graphene nanocomposites: $Al_2O_3$ graphene, RSC Adv., 4 (2014) 7418–7424.

[16] M.S.A. Bhuyan, M.N. Uddin, M.M. Islam, F.A. Bipasha, S.S. Hossain, Synthesis of graphene, Int. Nano Lett., 6 (2016) 65–83.

[17] J.A. Prince, S. Bhuvana, V. Anbharasi, N. Ayyanar, K.V.K. Boodhoo, G. Singh, Ultra-wetting graphene-based PES ultrafiltration membrane – A novel approach for successful oil-water separation, Water Res., 103 (2016) 311–318.

[18] H. Ha, C.J. Ellison, Polymer/graphene oxide (GO) thermoset composites with GO as a crosslinker, Korean J. Chem. Eng., 35 (2018) 303–317.

[19] R. Kumar, A.F. Ismail, Fouling control on microfiltration/ultrafiltration membranes: effects of morphology, hydrophilicity and charge, J. Appl. Polym. Sci., 132 (2015) 42042, (1–20) doi: 10.1002/app.42042.

[20] J. Zhang, Z. Xu, W. Mai, C. Min, B. Zhou, M. Shan, Y. Li, C. Yang, Z. Wang, X. Qian, Improved hydrophilicity, permeability, antifouling and mechanical performance of PVDF composite ultrafiltration membranes tailored by oxidized low-dimensional carbon nanomaterials, J. Mater. Chem. A, 1 (2013) 3101–3111.

[21] D. Han, L. Yan, W. Chen, W. Li, Preparation of chitosan/graphene oxide composite film with enhanced mechanical strength in the wet state, Carbohydr. Polym., 83 (2011) 653–658.

[22] D. Rana, K. Bag, S.N. Bhattacharyya, B.M. Mandai, Miscibility of poly(styrene-co-butyl acrylate) with poly(ethyl methacrylate): existence of both UCST and LCST, J. Polym. Sci., 38 (2000) 369–375.

[23] D. Rana, B.M. Mandal, S.N. Bhattacharyya, Analogue calorimetric studies of blends of poly(vinyl ester)s and polyacrylates, Macromolecules, 29 (1996) 1579–1583.

[24] D. Rana, B.M. Mandal, S.N. Bhattacharyya, Miscibility and phase diagrams of poly(phenyl acrylate) and poly(styrene-co-acrylonitrile) blends, Polymer, 34 (1993) 1454–1459.

[25] C. Liao, P. Yu, J. Zhao, L. Wang, Y. Luo, Preparation and characterization of NaY/PVDF hybrid ultrafiltration membranes containing silver ions as antibacterial materials, Desalination, 272 (2011) 59–65.

[26] Y.H. Zhao, B.K. Zhu, L. Kong, Y.Y. Xu, Improving hydrophilicity and protein resistance of poly(vinylidene fluoride) membranes by blending with amphiphilic hyperbranched-star polymer, Langmuir, 23 (2007) 5779–5786.

[27] Y. Chang, Y.J. Shih, R.C. Ruaan, A. Higuchi, W.Y. Chen, J.Y. Lai, Preparation of poly(vinylidene fluoride) microfiltration membrane with uniform surface copolymerized poly(ethylene glycol) methacrylate and improvement of blood compatibility, J. Membr. Sci., 309 (2008) 165–174.
[28] Y. Chen, Q. Deng, J. Xiao, H. Nie, L. Wu, W. Zhou, B. Huang, Controlled grafting from poly(vinylidene fluoride) microfiltration membranes via reverse atom transfer radical polymerization and antifouling properties, Polymer, 48 (2007) 7604–7613.
[29] M.A. Aroon, A.F. Ismail, T. Matsuura, M.M.M. Rahmati, Performance studies of mixed matrix membranes for gas separation: a review, Sep. Purif. Technol., 75 (2010) 229–242.
[30] X. Yang, H. Sun, A. Pal, Y. Bai, L. Shao, Biomimetic silicification on membrane surface for highly efficient treatments of both oil-in-water emulsion and protein wastewater, ACS Appl. Mater. Interfaces, 10 (2018) 29982–29991.
[31] X. Liu, H. Yuana, C. Wang, S. Zhang, L. Zhang, X. Liu, F. Liu, X. Zhub, S. Rohanic, C. Ching, J. Lu, A novel PVDF/PFSA-g-GO ultrafiltration membrane with enhanced permeation and antifouling performances, Sep. Purif. Technol., 233 (2020) 116038 (1–12), doi: 10.1016/j.seppur.2019.116038.
[32] K.Z. Riahi, N. Sdiri, D.J. Ennigrou, K.H. Naifer, Investigations on electrical conductivity and dielectric properties of graphene oxide nanosheets synthetized from modified Hummer's method, J. Mol. Struct., 1216 (2020) 128304 (1–9), doi: 10.1016/j.molstruc.2020.128304.
[33] E. Yang, H.E. Karahan, K. Goh, C.Y. Chuah, R. Wang, T.H. Bae, Scalable fabrication of graphene-based laminate membranes for liquid and gas separations by crosslinking-induced gelation and doctor-blade casting, Carbon,155 (2019) 129–137.
[34] A.C. Ferrari, J.C. Meyer, V. Scardaci, C. Casiraghi, M. Lazzeri, F. Mauri,S. Piscanec, D. Jiang, K.S. Novoselov, S. Roth, A.K. Geim, Raman spectrum of graphene and graphene layers, Phys. Rev. Lett., 97 (2006) 187401–187404.
[35] M. HagosKahsay, N. Belachew, A. Tadesse, K. Basavaiah, Magnetite nanoparticle decorated reduced graphene oxide for adsorptive removal of crystal violet and antifungal activities, RSC Adv., 10 (2020) 34916–34927.
[36] N. Wang, J. Wang, J. Zhao, J. Wang, J. Pan, J. Huang, Synthesis of porous-carbon@reducedgraphene oxide with superior electrochemical behaviors for lithium-sulfur batteries, J. Alloys Compd., 851 (2021) 156832 (1–10), doi: 10.1016/j.jallcom.2020.156832.
[37] C. Ma, J. Hu, W. Sun c, Z. Ma, W. Yang, L. Wang, Z. Ran, B. Zhao, Z. Zhang, H. Zhang, Graphene oxide-polyethylene glycol incorporated PVDF nanocomposite ultrafiltration membrane with enhanced hydrophilicity, permeability, and antifouling performance, Chemosphere, 253 (2020) 126649 (1–10), doi: 10.1016/j.chemosphere.2020.126649.
[38] A.M. Ismail, M.I. Mohammed, S.S. Fouad, Optical and structural properties of polyvinylidene fluoride (PVDF)/reduced graphene oxide (RGO) nanocomposites, J. Mol. Struct., 1170 (2018) 51–59.
[39] M. Mertens, T.V. Dyck, C.V. Goethem, A.Y. Gebreyohannes, I.F.J. Vankelecom, Development of a polyvinylidenedifluoride membrane for nanofiltration, J. Membr. Sci., 557 (2018) 24–29.
[40] H.H. Chang, L.K. Chang, C.D. Yang, D.J. Lin, L.P. Cheng, Effect of polar rotation on the formation of porous poly(vinylidene fluoride) membranes by immersion precipitation in an alcohol bath, J. Membr. Sci., 513 (2016) 186–196.
[41] M. Tao, F. Liu, B. Ma, L. Xue, Effect of solvent power on PVDF membrane polymorphism during phase inversion, Desalination, 316 (2013) 137–145.
[42] Z. Zhu, L. Wang, Y. Xu, Q. Li, J. Jiang, X. Wang, Preparation and characteristics of graphene oxide-blending PVDF nanohybrid membranes and their applications for hazardous dye adsorption and rejection, J. Colloid Interface Sci., 504 (2017) 429–439.
[43] R. Gregorio, Determination of the $\alpha$, $\beta$, and $\gamma$ crystalline phases of poly(vinylidene fluoride) films prepared at different conditions, J. Appl. Polym. Sci., 100 (2006) 3272–3279.
[44] M.C. Branciforti, V. Sencadas, S.L. Mendez, R. Gregorio, New technique of processing highly oriented poly(vinylidene fluoride) films exclusively in the $\beta$ phase, J. Polym. Sci., Part B: Polym. Phys., 45 (2007) 2793–2801.
[45] H. Yu, L. Gu, S. Wu, G. Dong, X. Qiao, K. Zhang, X. Lu, H. Wen, D. Zhang, Hydrothermal carbon nanospheres assisted-fabrication of PVDF ultrafiltration membranes with improved hydrophilicity and antifouling performance, Sep. Purif. Technol., 247 (2020) 116889 (1–11), doi: 10.1016/j.seppur.2020.116889.
[46] K.J. Nakanishi, Infrared adsorption spectroscopy, practical, Holden-Day, 79 (1962) 392.